Materials Today Bio 23 (2023) 100864

Contents lists available at ScienceDirect

Materials Today Bio

journal homepage: www.journals.elsevier.com/materials-today-bio

Injectable hydrogel with selenium nanoparticles delivery for sustained glutathione peroxidase activation and enhanced osteoarthritis therapeutics

Wenhui Hu [a,1], Xuan Yao [a,b,1], Yuheng Li [a], Jianmei Li [a], Jing Zhang [c], Zhi Zou [c], Fei Kang [a,**], Shiwu Dong [a,d,*]

[a] Department of Biomedical Materials Science, College of Biomedical Engineering, Army Medical University (Third Military Medical University), Chongqing, PR China
[b] Department of Clinical Hematology Faculty of Laboratory Medicine, Army Medical, University (Third Military Medical University), Chongqing, PR China
[c] College of Bioengineering, Chongqing University, Chongqing, PR China
[d] State Key Laboratory of Trauma and Chemical Poisoning, Army Medical University (Third Military Medical University), Chongqing, PR China

ARTICLE INFO

Keywords:
Selenium metabolism
Injectable hydrogel
Osteoarthritis
Selenium nanoparticles
Glutathione peroxidase-1

ABSTRACT

Reactive oxygen burst in articular chondrocytes is a major contributor to osteoarthritis progression. Although selenium is indispensable role in the antioxidant process, the narrow therapeutic window, delicate toxicity margins, and lack of an efficient delivery system have hindered its translation to clinical applications. Herein, transcriptomic and biochemical analyses revealed that osteoarthritis was associated with selenium metabolic abnormality. A novel injectable hydrogel to deliver selenium nanoparticles (SeNPs) was proposed to intervene selenoprotein expression for osteoarthritis treatment. The hydrogels based on oxidized hyaluronic acid (OHA) cross-linked with hyaluronic acid-adipic acid dihydrazide (HA-ADH) was formulated to load SeNPs through a Schiff base reaction. The hydrogels were further incorporated with SeNPs, which exhibited minimal toxicity, mechanical properties, self-healing capability, and sustained drug release. Encapsulated with SeNPs, the hydrogels facilitated cartilage repair through synergetic effects of scavenging reactive oxygen species (ROS) and depressing apoptosis. Mechanistically, the hydrogel restored redox homeostasis by targeting glutathione peroxidase-1 (GPX1). Therapeutic outcomes of the SeNPs-laden hydrogel were demonstrated in an osteoarthritis rat model created by destabilization of the medial meniscus, including cartilage protection, subchondral bone sclerosis improvement, inflammation attenuation, and pain relief were demonstrated. These results highlight therapeutic potential of OHA/HA-ADH@SeNPs hydrogels, providing fundamental insights into remedying selenium imbalance for osteoarthritis biomaterial development.

1. Introduction

Degenerative joint diseases, such as osteoarthritis, cause chronic pain, physical disability, and impose a substantial financial burden on medical insurance [1,2]. Inflammatory cytokines play a significant role in the pathogenesis of osteoarthritis by promoting cartilage degradation. They induce the generation of large amounts of reactive oxygen species, mitochondrial damage, and chondrocyte catabolism and apoptosis. These processes contribute to the progression of osteoarthritis [3–5]. Due to the lack of comprehensive understanding regarding the molecular mechanisms and pathways that involved in osteoarthritis and the poor self-repair capacity of cartilage, osteoarthritis remains a challenging disease in spite of limited therapeutic options [6]. Currently, most of the treatment approaches are only effective in achieving pain relief rather than reversing the cartilage damage [7,8]. Clinical therapies of osteoarthritis approaches are divided into physical modalities, pharmacologic treatments, and surgical treatments. The following classes of drugs are currently used to treat osteoarthritis: non-steroidal anti-inflammatory drugs (NSAIDs), glucocorticoids, opioids, symptomatic, chondroprotective agents, and anticytokines [9]. Despite the localized nature of osteoarthritis, intra-articular therapeutic of FDA-approved hyaluronate formulations and corticosteroids face

* Corresponding author. Department of Biomedical Materials Science, College of Biomedical Engineering, Army Medical University (Third Military Medical University), Chongqing, PR China.
** Corresponding author.
E-mail addresses: kangfeilove2007@126.com (F. Kang), dongshiwu@163.com (S. Dong).
[1] The first two authors (Wenhui Hu and Xuan Yao) contributed equally to this work.

https://doi.org/10.1016/j.mtbio.2023.100864
Received 20 June 2023; Received in revised form 24 October 2023; Accepted 10 November 2023
Available online 11 November 2023

several challenges, such as short half-life, rapid clearance, and frequent requirement for administration and related side effects [10]. Therefore, developing alternative management strategies is of great importance.

The human body operates as a highly intricate and finely tuned system, and any disruption of its balance can lead to illness, as demonstrated by conditions like hypovitaminosis and iron-deficiency anemia [11,12]. Selenium is an essential nutritive and trace element vital to redox homeostasis and exerts its physiological role through selenoproteins containing selenocysteine (Sec) at their active sites [13,14]. Deficiency of selenium leads to oxidative stress that negatively impacts joint development. It has been established that selenium deficiency is the primary cause of endemic Kashin-Beck disease in low-selenium areas (mainly including the Siberian region of Russia, China, and North Korea) [15,16]. Moreover, the association between selenium metabolism and skeletal pathologies has been generally acknowledged in the context of the beneficial effects on selenium as a nutritional supplement in various clinical and animal studies [17,18]. The underlying mechanism by which the dysregulation of selenium nutrient balance occurs during osteoarthritis remains unclear. Based on the role of selenium metabolism in redox regulation, we hypothesized that selenium supplementation might be a promising therapeutic strategy for ameliorating osteoarthritis development.

Although selenium is widely used in nutritional supplements, it has a narrow therapeutic window and delicate toxicity margins [19]. Intriguingly, selenium nanoparticles (SeNPs) are alternatives for dietary supplementation due to the higher biocompatibility than those of the organic and inorganic forms of selenium [20]. SeNPs have received extensive attention due to their excellent biocompatibility, antibacterial, antiviral, and anticancer activities, and fight against large amounts of reactive oxygen species (ROS) and proinflammatory cytokines, the major etiological factors for osteoarthritis [21,22]. Meanwhile, compared to traditional antioxidant drugs, SeNPs exhibit the properties of some natural antioxidant enzymes (nanozymes), such as selenoproteins, including glutathione peroxidases (GPXs), and have outstanding advantages over natural enzymes due to their modifiable physicochemical properties, high biostability, and diverse catalytic activities [21,23–26]. As nanoparticles have non-negligible concentration-dependent therapeutic effects and articular cartilage is an avascular tissue, the systemic delivery strategy may results in low residual concentration of drugs in the joint and cause poor therapeutic effects [27]. To obtain long-term effects, repeated multiple injections becomes necessary, while irreparable cartilage damage caused by excessive injections seriously limits its application. In addition to other traditional intra-articular injection formulations, nanomaterials, including selenium nanoparticles, are also characterized by a short retention time within the joint, which restricts their utilization. The short half-life of these nanoparticles necessitates more frequent administrations or higher loading concentrations, which can increase potential toxicity and the cost associated with their use [28–31].

In recent years, hydrogel delivery platforms have gained attention due to their potential for localized, prolonged, and sustained release of therapeutics to target tissues [27]. Among various types of novel intra-articularly injectable materials, hyaluronic acid hydrogels are often prioritized due to the high biocompatibility and physical and chemical properties resembling human tissues [32]. However, a significant challenge in osteoarthritis treatment arises from the lack of self-healing capability in some injectable hydrogels. The joint space experiences high local stress, which can cause these hydrogels to break into small fragments, potentially leading to premature release or leakage of the encapsulated drug [27]. Indeed, an the ideal crosslinked hydrogel carrier delivery SeNPs should be injectable for minimally invasive purpose, possess self-healing to resist breakage, and exhibit sustained SeNPs release for a prolonged therapeutic effect.

This work analyzed the selenium metabolic pathway under osteoarthritis conditions based on multiple transcriptomic data. Biochemical analyses indicated that rats in a destabilized medial meniscus (DMM) model of osteoarthritis exhibited lower levels of serum selenium and glutathione peroxidase (GSH-PX). Based on the understanding that selenium plays a role in regulating redox homeostasis and cartilage degeneration in osteoarthritis by inducing selenoproteins, an in situ injectable and self-healing hydrogel delivery platform was designed in our study. The purpose of this platform was to transport selenium nanoparticles for sustained manipulation of selenoproteins and to enhance the therapy of osteoarthritis. This hydrogel was conveniently fabricated by one-step mixing of the oxidized hyaluronic acid (OHA) solution with adipic dihydrazide-grafted HA (HA-ADH) solution and selenium nanoparticles (SeNPs) suspension to form OHA/HA-ADH@SeNPs based on the mild Schiff base reaction between OHA and HA-ADH and the dispersion of SeNPs in the gel network. By utilizing the self-healing capability of Schiff base bonds, our hydrogel dressing could achieve the "Package firstly, injection when needed" concept, which aligns with the requirements for commercialization [33–36]. The encapsulated selenium nanoparticles within the hydrogel network could be released in response to exposure to a weakly acidic inflammatory microenvironment. The hydrogels allow for on-demand release of the SeNPs, providing targeted and timely therapeutic intervention. Finally, OHA/HA-ADH@SeNPs-gel could provide sustained glutathione peroxidase-1 (GPX1) activation and antioxidation for the therapy of cartilage injury in the DMM-induced rat osteoarthritis model, as shown in Scheme 1.

2. Materials and methods

2.1. Materials

Hyaluronic acid (HA, Mw: 10–50 kDa) was obtained from Focusfreda Biotech Co. Ltd (Shanghai, China). Sodium periodate (SP) and morpholine ethane sulfonic acid buffer (MES buffer, pH = 6.5) were obtained from Shanghai Macklin Biochemical Technology Co. Ltd. N-(3-Dimethylaminopropyl)-N′-ethyl carbodiimide hydrochloride (EDC) was purchased from Aladdin Industrial Co. Ltd (Shanghai, China). Hydroxybenzotriazole (Hobt, 99 %) was obtained from Mindray Chemical Technology Co. Ltd (Shanghai, China), and oxalyl dihydrazide (ADH) was obtained from J&K Scientific (Beijing, China). Selenium nanoparticles (SeNPs) were purchased from Feynman Nano (Zhengzhou, China). Penicillin-streptomycin, trypsin-EDTA, and fetal bovine serum (FBS) were obtained from Gibco (Carlsbad, CA). CCK-8 kit, Live/Dead kit, Hoechst, and 4′,6-diamidino-2-phenylindole (DAPI), were acquired from Beyotime (Shanghai, China). SW1353 cells were obtained from the National Collection of Authenticated Cell Cultures (Shanghai, China). L-15 Dulbecco's modified Eagle medium was obtained from Saibaikang (Shanghai, China). Lipofectamine 3000 siRNA transfection system was obtained from (Invitrogen; L3000015). Negative control siRNA and si-GPX1 were purchased from Paivi Biotechnology Co., Ltd. (Wuhan, China) and the siRNA sequences were showed in Table S2.

2.2. Synthesis and characterization of OHA and HA-ADH hydrogel

OHA was fabricated according to the sodium periodate oxidation method [37]. Briefly, 1g of HA was dissolved in 100 mL water, into which 0.3g SP was added. The reaction was magnetically stirred for 24 h at room temperature in the dark. To stop the oxidation reaction, diethylene glycol was added in an equimolar amount. One hour later, the mixture underwent exhaustive dialysis for 3 days against water. The oxidation degree of HA was confirmed by detecting the aldehyde content via the hydroxylamine hydrochloride titration method [38].

HA-ADH was fabricated via a carboxyl-amino reaction under the catalysis of HOBt and EDC [39]. Briefly, 1g of HA was dissolved in 100 mL of MES buffer (pH = 6.5), and EDC (1.25 g) and HOBt (0.89 g) were added sequentially for 1 h. Then, 4.5g ADH was added for another 24 h at room temperature. After the above reaction was complete, the mixture was dialyzed exhaustively for 4 days against water. Fourier

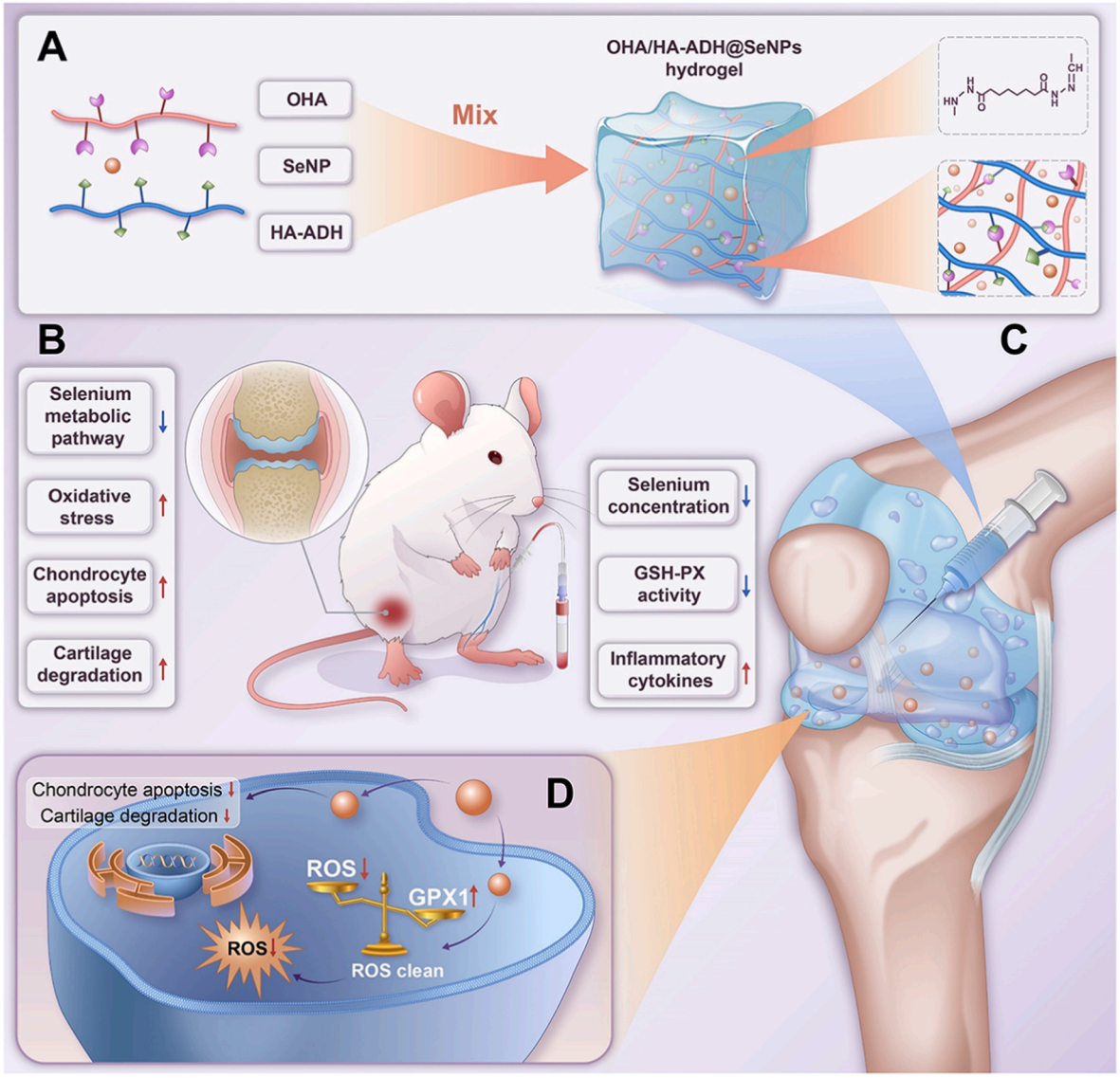

Scheme 1. Schematic demonstration of the synthesis of OHA/HA-ADH@SeNPs-gels with multifunctional properties for potential application in repairing osteoarthritic cartilage damage. (A) Schematic diagram of OHA/HA-ADH-gels synthesis. With their remarkable versatility and favorable chemical, biological and mechanical properties, OHA/HA-ADH-gels exhibit the desired release profile by encapsulating SeNPs in their porous structure. (B) Selenium deficiency, disturbances of oxidant balance, cartilage degradation, and inflammatory cytokines are overexpressed in osteoarthritis. (C) The injectable crosslinked OHA/HA-ADH-gels developed as an intra-articular delivery platform for sustainably releasing SeNPs in the inflamed joint. (D) The OHA/HA-ADH@SeNPs-gels inhibited cartilage matrix degeneration through synergetic effects of redox homeostasis restoration and inhibiting apoptosis by targeting GPX1 that catalyzed oxidative damage.

transform infrared spectroscopy (FTIR, Thermo Scientific Nicolet 6700) and ^{1}H nuclear magnetic resonance (NMR, Bruker DMX, 400 MHz) were used to characterize their chemical structures.

2.3. Preparation of OHA/HA-ADH@SeNPs hydrogel

The hydrogel was prepared with equal volumes of 2 % (w/w) OHA and 2 % (w/w) HA-ADH. The concentration of SeNPs in the hydrogels was 100 μg/mL. The obtained hydrogels were washed three times with deionized water, followed by freezing at −80 °C, lyophilized and stored at 4 °C.

2.4. Gelation time, scanning electron microscopy (SEM), and swelling ratio assay

The gelation times were determined as previously reported [40]. 500 μL OHA was put into a penicillin bottle under continuous stirring at 100 rpm. 500 μL of HA-ADH was then added to the bottle. The mixture was stirred until it became a solid, which was the gelation time. After gelation, the hydrogel samples were freeze-dried followed by underwent critical point drying and gold sputter coating. At least three random views were captured for analysis. For the swelling assay, a lyophilized hydrogel (weighted as W_0) was immersed in PBS (pH = 7.4) at 37 °C for 24 h to ensure the hydrogel reached its equilibrium swelling state. Then, the hydrogel was withdrawn from PBS and removed excess water. Its weight was recorded as Ww. The swelling ratio (SR) was calculated by the formula: $SR = (W_w\text{-}W_0)/W_w \times 100\ \%$.

2.5. Rheological test of hydrogel

The dynamic rheological experiments of hydrogels were determined using a rheometer (Anton Paar MCR 302, Austria) at room temperature. Hydrogel (1 mL) was placed on a parallel plate (20 mm). The storage modulus (G') and loss modulus (G'') were measured by time sweep

experiments using a fixed train of 1 % and a frequency of 1 Hz. To detect the critical strain point in hydrogels, the strain amplitude sweep test was used at a fixed frequency of 1 Hz with a strain ranging from 0.1 % to 1000 %. To confirm the self-healing ability of hydrogels, the continuous step-strain test was conducted. In brief, the oscillatory strain was alternated between a small strain of 1 % and a large strain of 300 % at a fixed frequency of 1 Hz, keeping a duration of 120 s for each step. To observe the injectability of OHA/HA-ADH@SeNPs hydrogel, a trace amount of dye that does not react with the hydrogel was applied for better visualization. The hydrogel was placed in a syringe with a 26-gauge needle and then injected through a needle directly on a plate. Two pieces of hydrogels dyed pink and blue were put together and merged into a single integral hydrogel again without any external stimulus to further illustrate its self-healing performance.

2.6. Cells culture and osteoarthritis cell model

SW1353 cells were cultured in L-15 Dulbecco's modified Eagle medium at 37 °C in 5 % CO_2. To assess the anti-osteoarthritic effects of the hydrogel, OHA/HA-ADH@SeNPs hydrogels were immersed in the culture medium for 5 days, and the extract was collected for subsequent cell experiments. IL-1β is widely used to induce an osteoarthritis-like response [41]. In this study, SW1353 cells were exposed to 40 ng/mL recombinant human IL-1β (R&D) and cultured with the above leaching solution or normal culture medium.

2.7. RNA isolation and real-time PCR

Total RNA was extracted by lysing the cells using RNAiso Plus (Takara, Shiga, Japan) according to the manufacturer's protocol. The mRNA was reverse transcribed using PrimeScript RT Master Mix (Takara, Shiga, Japan). The synthesized cDNA was amplified by TB Green™ Premix Ex Taq™ (Takara, Shiga, Japan). The human-specific primer sequences were synthesized by Sango Biotech (Shanghai, China). The sequences of the primers are showed in Table S3, Supporting Information. The Ct value of the target gene was normalized to the endogenous control GAPDH, and the relative expression levels were calculated using the $2^{-\Delta\Delta Ct}$ method.

2.8. Immunofluorescence staining

Cells were fixed in 4 % paraformaldehyde for 30 min at room temperature and then 0.1 % Triton X-100 was added for 30 min. Cells were incubated with the anti-MMP13 (Bioworld Technology, BS90868, 1:200), anti-COLII (Bioss, bs-10589R, 1:100), anti-GPX1 (Beyotime, AF7017, 1:100), or anti-cleaved caspase-3 (Beyotime, AF1150, 1:100) primary antibodies at 4 °C overnight. Then, the cells were washed with PBS and incubated with Cy3-conjuwgated goat anti-rabbit IgG or FITC-conjugated goat anti-rabbit IgG (Servicebio, China) for 1 h at room temperature. The nuclei were counterstained with DAPI for 10 min, and the immunofluorescence images were visualized using a fluorescence microscope (Bio-Rad, USA).

2.9. Rat model of osteoarthritis

Male SD rats (with an average age of 12 weeks) were purchased from Charles River Corporation (Beijing, China). Surgical destabilization of the medial meniscus (DMM) was used to prepare the osteoarthritis model [42]. In order to anesthetize the rats, 40 mg/kg of pentobarbital was injected intraperitoneally. An incision was made from the distal patella of the right knee joint up to the proximal tibial plateau, the right knee joint was fully exposed, and the medial meniscus tibial ligament (MMTL) was severed with a scalpel for better separation of the medial meniscus. A microvascular forceps was then used to remove the meniscus and layers of sutures were applied to the incision. Sham operations were conducted in the same way, except that the MMTL was not cut. A horizontal treadmill was used to induce knee osteoarthritis in rats by making them run at 20 m/min for 30 min/day 3 days a week in four random groups. 100 μL of PBS, OHA/HA-ADH, and OHA/HA-ADH@SeNPs hydrogels were injected into the joint cavity of each rat. All operations were performed under National Institutes of Health guidelines. The experiment was approved by the Ethics Committee of Army Medical University.

2.10. Microcomputed tomography analysis

Microcomputed tomography (Bruker, Belgium) was used to reconstruct the knee joints that were scanned after being fixed in 70 % ethanol overnight. and CT reconstruction software (NRecon v1.6). The X-ray images were taken to measure the joint space widths (JSWs). Then, CTAn v1.9 and CTVol v2.0 were used for three-dimensional model visualization and further data analysis. The scanner parameters were 50 kV voltage, 200 μA current, and 9 μm per pixel resolution. The entire subchondral bone of the specimens was selected as the region of interest. Tb.Th, Tb.N, BV/TV, and Tb.Sp were measured.

2.11. Detection of inflammatory cytokines

The cytokine antibody array (Wayen Biotechnology Co. Ltd., Shanghai, China) was used to detect inflammatory cytokines in serum samples obtained from rats 8 weeks post DMM surgery. Different fluorescently labeled magnetic beads were coupled to highly specific capture monoclonal antibodies in the cytokine antibody array. Different magnetic beads were mixed and suspended in a 96-well microplate. A biotin-labeled high-affinity paired detection antibody was added to enhance cytokine detection signals. Then, the normalized signal value was normalized between samples using a positive control. Finally, the normalized data were used for intergroup comparisons.

2.12. Gait acquisition

The right feet of the rats were stained with red ink, and the left feet were stained with blue ink. Then, the rats were guided to walk naturally on the paper to collect footprints. At least 4–6 footprints were from each rat for data analysis. Generally, the first few footprints are not included in statistical analysis, and the rat may not be in continuous walking at this time.

2.13. Histologic and immunohistochemical examinations

After 8 weeks of modeling, the knee joints were fixed, decalcified, embedded, and sagittally sectioned (5 μm). Hematoxylin and eosin (H&E) and Safranin O-fast green staining were performed for histological analysis. Three blinded observers evaluated the pathology scores of each picture. For immunohistochemical staining, anti-COLII (Servicebio, GB11021, 1:200), anti-MMP13 (Servicebio, GB11247, 1:100), anti-GPX1 (BOSTER, M01019-2, 1:100) or anti-TNF-α (Bioworld Technology, BS6000, 1:200), anti-IL-1β (Bioworld Technology, BS65005, 1:200) primary antibodies were used to incubate the sections overnight at 4 °C. Then, the sections were incubated with goat anti-rabbit secondary antibodies for 1 h and reacted with DAB. Image J 1.46r software was used to quantify the relative expressions (Wayne Rasband, NIH, USA).

2.14. Statistical analysis

All the data were analyzed using a specific software (GraphPad Prism 9.0), and data were expressed as means ± standard deviation. The p value < 0.05 was statistically significant. Student's t-tests were used to analyze the significance of differences between the two groups. For pairwise comparisons, the differences among multiple groups were assessed using a one-way ANOVA followed by a Tukey post-hoc test.

3. Results and discussion

3.1. Selenium metabolic abnormality and oxidative stress damage associated with osteoarthritis development

To investigate the pathological changes in osteoarthritis, transcriptome sequencing was performed to disclose the underlying mechanisms that lead to osteoarthritis in human or rat cartilage. Dysregulated extracellular matrix (ECM) metabolism, for example, ECM-receptor interaction and protein digestion and absorption, has been associated with osteoarthritis progression. Enrichment analysis indicated that oxidative stress (cellular response to reactive oxygen species (ROS) and ROS metabolic process) and nutrient metabolism (cysteine metabolism and cellular modified amino acid metabolic process) were highly correlated (Fig. 1A–F and Figs. S1–S2). Selenium is an essential trace element incorporated into selenoproteins, taking the form of selenocysteine. We found that serum selenium level in osteoarthritis rats was significantly lower compared to control rats (Fig. 1G). Selenoproteins

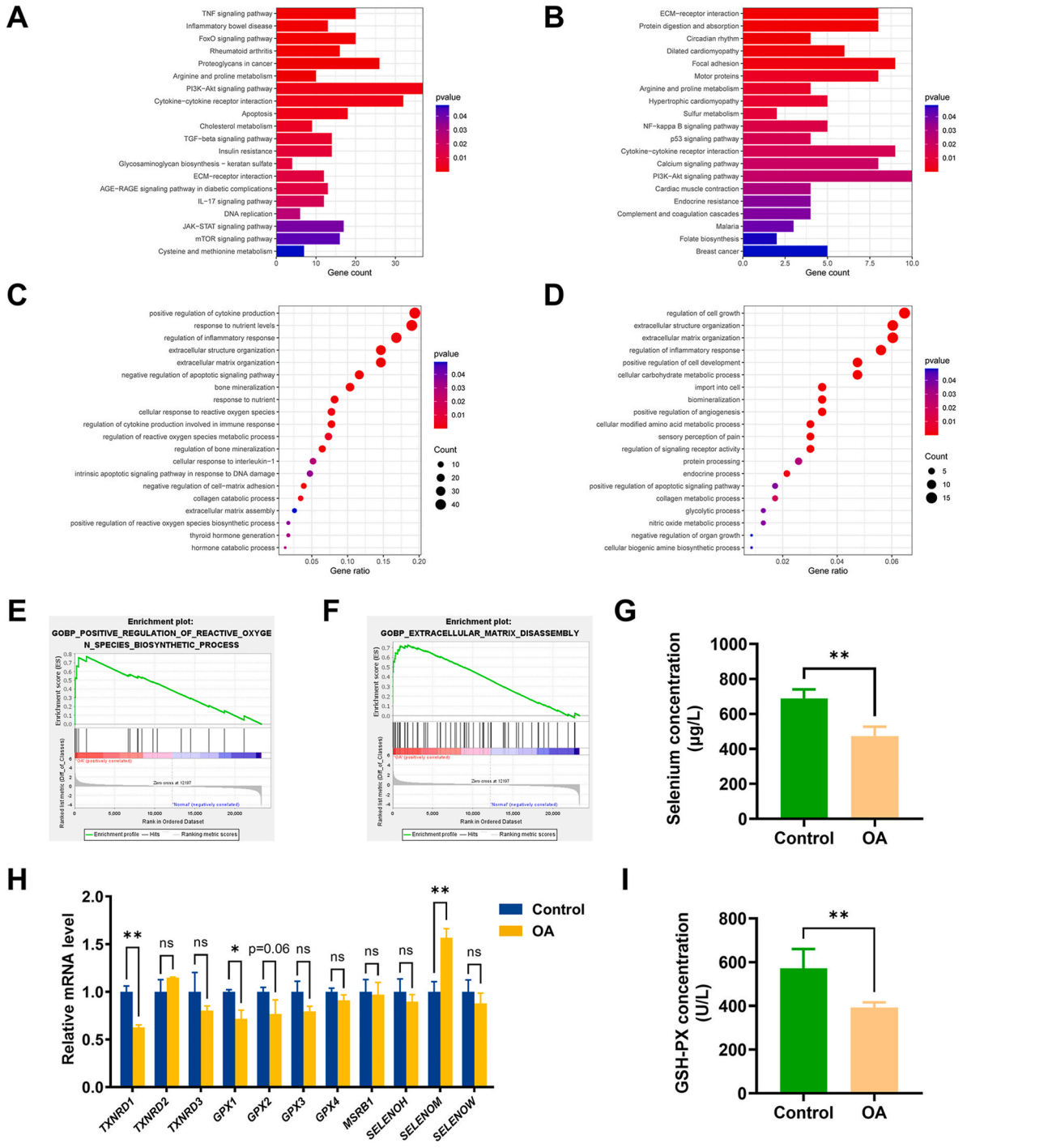

Fig. 1. Selenium status and oxidative stress in osteoarthritis conditions. (A–B) Kyoto Encyclopedia of Genes and Genomes (KEGG) enrichments based on database resources (GSE64394 and GSE8077). (C–D) Gene Ontology (GO) enrichments based on database resources (GSE64394 and GSE8077). (E–F) GSEA enrichment analysis identified the potential pathways of OA cartilage samples. (G) ICP-MS detected serum selenium concentrations of individuals with osteoarthritis and controls (n = 5 in each group). (H) Transcript levels of the selenoproteins were determined with RT-PCR assays. (I) ELISA detected serum GSH-PX activity of individuals with osteoarthritis and controls (n = 5 in each group). The results are shown as the mean ± SD. *, $p < 0.05$; **, $p < 0.01$.

play a crucial role in protecting against oxidative stress damage by acting as an important line of defense. Next, we compared transcriptional profiles of genes involved in the selenium metabolic pathway, the expression of selenoprotein genes was altered significantly in osteoarthritis transcriptome datasets (Fig. S3). Correspondingly, the expression of the well-characterized selenoproteins, including the members of the thioredoxin reductases, glutathione peroxidases and deiodinases gene families, was detected. The levels of GPXs and thioredoxin reductase 1 (TXNRD1) were altered at the mRNA level (Fig. 1H). Meanwhile, a significant decline was observed in the antioxidant activity of GSH-PX in osteoarthritis rats compared to in control rats (Fig. 1I). These results showed that selenium metabolic abnormality and oxidative stress damage were correlated with osteoarthritis progression.

3.2. Preparation and characterization of OHA and HA-ADH hydrogels

The OHA/HA-ADH@SeNPs hydrogels were prepared by mixing OHA with SeNPs, followed by reacting with HA-ADH via a Schiff base reaction (Fig. 2A). The successful synthesis of OHA was confirmed by Fourier transform infrared (FTIR) spectrum and proton nuclear magnetic resonance (^{1}H NMR). In contrast with the FTIR spectrum of HA, the characteristic peaks of HA were still present in OHA, whereas a new peak appeared at 1744 cm^{-1}, which was attributed to the stretching vibration of aldehyde groups (Fig. S4A). The presence of new peaks at 4.6 ppm and 5.1 ppm on the ^{1}H NMR spectrum provided further evidence of the successful synthesis of OHA (Fig. S4B). The hydroxylamine hydrochloride titration method was utilized to measure the content of aldehyde groups, indicating approximately 33.71 % of the aldehyde groups in each repeating unit of OHA (Table S1). The successful synthesis of HA-ADH was proved by the ^{1}H NMR (Fig. S5). Based on the integration ratio of the –CH_3 peak at 1.9 ppm in HA and the methylene proton peaks of ADH, the ADH substitution degree on HA was reckoned to be 40 %. This estimation was based on a previously reported and well-documented formula that allows for the determination of the degree of substitution in such systems [43,44].

3.3. Design, synthesis, and characterization of hydrogels for SeNPs delivery

The hydrogels were formed in phosphate buffer (PBS) (pH = 7.4) after uniformly mixing OHA (containing SeNPs) with HA-ADH (Fig. 2B). The lyophilized OHA/HA-ADH@SeNPs-gels possessed microporous structures, and their average pore size was 149.17 ± 14.79 μm (Fig. 2C), while the average pore size of lyophilized HA hydrogels is 143.77 ± 8.76 μm (Figs. S6A–B). The gelation time of the HA-SeNPs hydrogels was around 30s, which was similar to the HA hydrogels (Fig. S6C). The OHA/HA-ADH@SeNPs-gels showed a slightly lower swelling ratio than the HA hydrogels, and no significant difference was found between the two groups (Fig. S6D). The mechanical properties of the hydrogels were characterized with the uniaxial compression experiment. Fig. S7A presented the stress-strain curves of the OHA/HA-ADH and OHA/HA-ADH@SeNPs. Owing to the flexibility and deformability of the dynamic covalent bond network, no fracture occurred during the compression. The compression modulus of the OHA/HA-ADH and OHA/HA-ADH@SeNPs, which reflects their resistance to deformation, was 26.67 ± 5.77 kPa and 36.67 ± 11.55 kPa, respectively (Fig. S7B). The compressive strength of OHA/HA-ADH@SeNPs was 40.00 ± 17.32 kPa, which was considerable with OHA/HA-ADH (63.33 ± 25.17 kPa) (Fig. S7C).

The self-healing and injectable performance of OHA/HA-ADH@SeNPs-gels were using a macroscopic test and rheological recovery test. The strain amplitude sweeps, and continuous step strain tests were applied to estimate the self-healing property of the hydrogels. The G' (storage modulus) and G'' (loss modulus) curves intersected at a strain of approximately 230 %, indicating that the hydrogel network was disrupted (Fig. 2D). The continuous step strain tests were further performed according to the result. The amplitude oscillatory strains were alternated from a small strain of 1 % to a large train of 300 % with each interval lasting 120 s. In the presence of a high dynamic strain (300 %), G′ decreased and became lower than G″. Once the strain was turned to a low value (1 %), both G′ and G″ immediately returned to their original values in all cycles (Fig. 2E). As shown in Fig. S8, the composite hydrogel degraded over time and completely biodegradable within 8 days in an equilibrium solution (PBS) containing 100 U mL^{-1} hyaluronidase at 37 °C. These results indicated an outstanding biodegradable property of the hydrogel. With a longer duration, the Se release rate was slow with a completely release within 10 days (Fig. 2F). The release of SeNPs from the hydrogel was with a sustained rate, which makes it a desirable platform for a long-term Se release. It was possible to continuously inject hydrogels without clogging using a 26-gauge needle (Fig. 2G). As shown in Fig. 2H and I, two separated hydrogels with pink and blue colors were integrated into a new single and complete hydrogel. These injectable and self-healing properties endow the hydrogel with a potential for intra-articular injection and efficient energy dissipation in weight-bearing joints [45].

3.4. In vitro biocompatibility tests of OHA/HA-ADH@SeNPs hydrogels

The use of primary chondrocytes tends to be limited by heterogeneity in loss of phenotype, limited proliferative ability, and substantial changes in the gene expression pattern during *in vitro* culture. *In vitro* analytical experiments often use chondrocyte cell lines as a substitute [44,46]. Human chondrosarcoma-derived SW1353 cells exhibit sufficient proliferation capacity and a consistent response to phenotype. Therefore, SW1353 cell lines have been leveraged to explore mechanisms of joint inflammation and cartilage destruction in the functional studies of chondrocytes and related diseases [47,48]. In our study, this cell line was selected for the following cell experiments. The results showed that the groups with SeNPs concentration less than or equal to 5 μg/mL showed high cell viability close to 100 %. Among them, SeNPs can significantly promote cell proliferation (Fig. S9). The extracts were acquired by immersing 50 μL hydrogels in 1 mL complete medium at 37 °C. Therefore, the SeNPs concentration in the hydrogel containing SeNPs was fixed as 100 μg/mL. Indeed, as implantable lubricating biomaterials, the SeNPs-incorporating HA-based hydrogels (OHA/-HA-ADH@SeNPs) should be biocompatible. The Live/Dead assay results showed that almost all cells were alive after 3 days of culture, with no significant differences between the groups (Fig. 3A). Similarly, the results of Live/Dead assay and the CCK-8 assay showed that the number of SW1353 cells in each group increased over time without significant an inter-group difference (Fig. 3B). Overall, the above results demonstrated that the OHA/HA-ADH@SeNPs have favorable biocompatibility and can be harnessed to exert chondroprotective effects *in vitro*.

3.5. Protective effects on celluar homeostasis maintenance

The accumulation of ROS can lead to oxidative stress damage in cells, eventually resulting in diseases such as osteoarthritis [49]. Considering especially focused on exploring the ROS depletion efficacy of hydrogels for SeNPs delivery, the leaching solution of the SeNPs-loaded hydrogels was cultured with IL-1β-stimulated SW1353 cells. The protective effect of hydrogels on SW1353 cells against the excess ROS was also evaluated. A ROS probe, dichloro-dihydro-fluorescein diacetate was applied to detect the intracellular ROS variations. As shown in Fig. 3C, the intracellular ROS level was significantly lower in the OHA/HA-ADH@SeNPs group than in the HA and blank groups, indicating that OHA/HA-ADH@SeNPs could reduce ROS generation by delivering SeNPs.

It is well-established that excessive production of ROS can promote chondrocyte damage, resulting in the biodegradation of extracellular matrix, and levels of matrix-degrading enzymes contribute significantly to matrix degradation in osteoarthritis cartilage [49]. To determine the

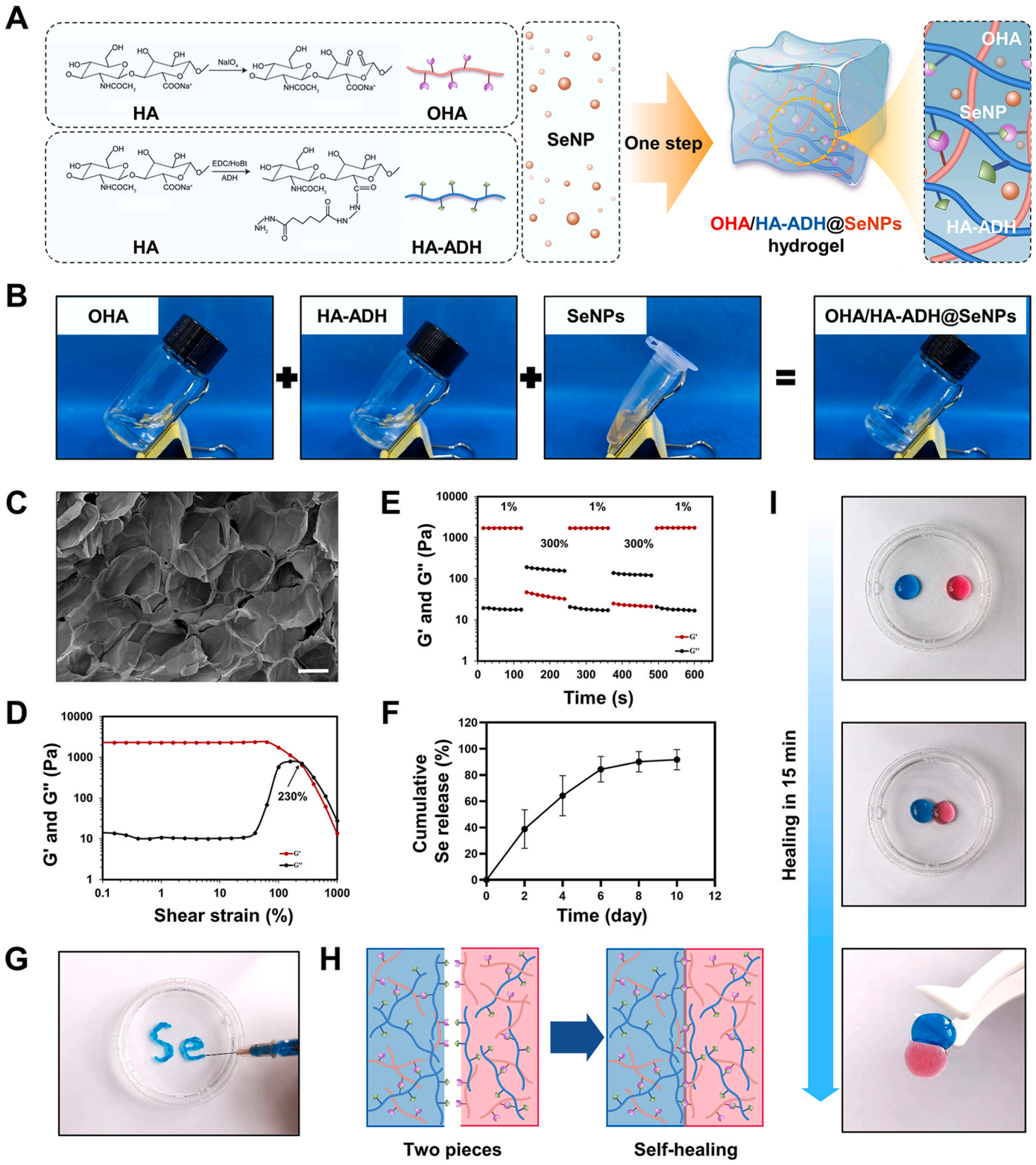

Fig. 2. The formation and characterization of OHA/HA-ADH@SeNPs hydrogel. (A) Schematic diagram of the synthesis of OHA/HA-ADH@SeNPs hydrogel. (B) The gelation process images of OHA/HA-ADH@SeNPs hydrogel. (C) SEM analysis of the lyophilized hydrogel structure. (D) Strain amplitude sweep test of the hydrogel at a fixed shear frequency of 1 Hz. (E) Step strain test of the hydrogel at a fixed shear frequency of 1 Hz. (F) SeNPs releasing curves of the OHA/HA-ADH@SeNPs hydrogel. (G) Images of OHA/HA-ADH@SeNPs hydrogel injected from a 26-gauge needle without clogging. (H) Schematic of the self-healing mechanism. (I) Macroscopic image showing the hydrogel's self-healing properties.

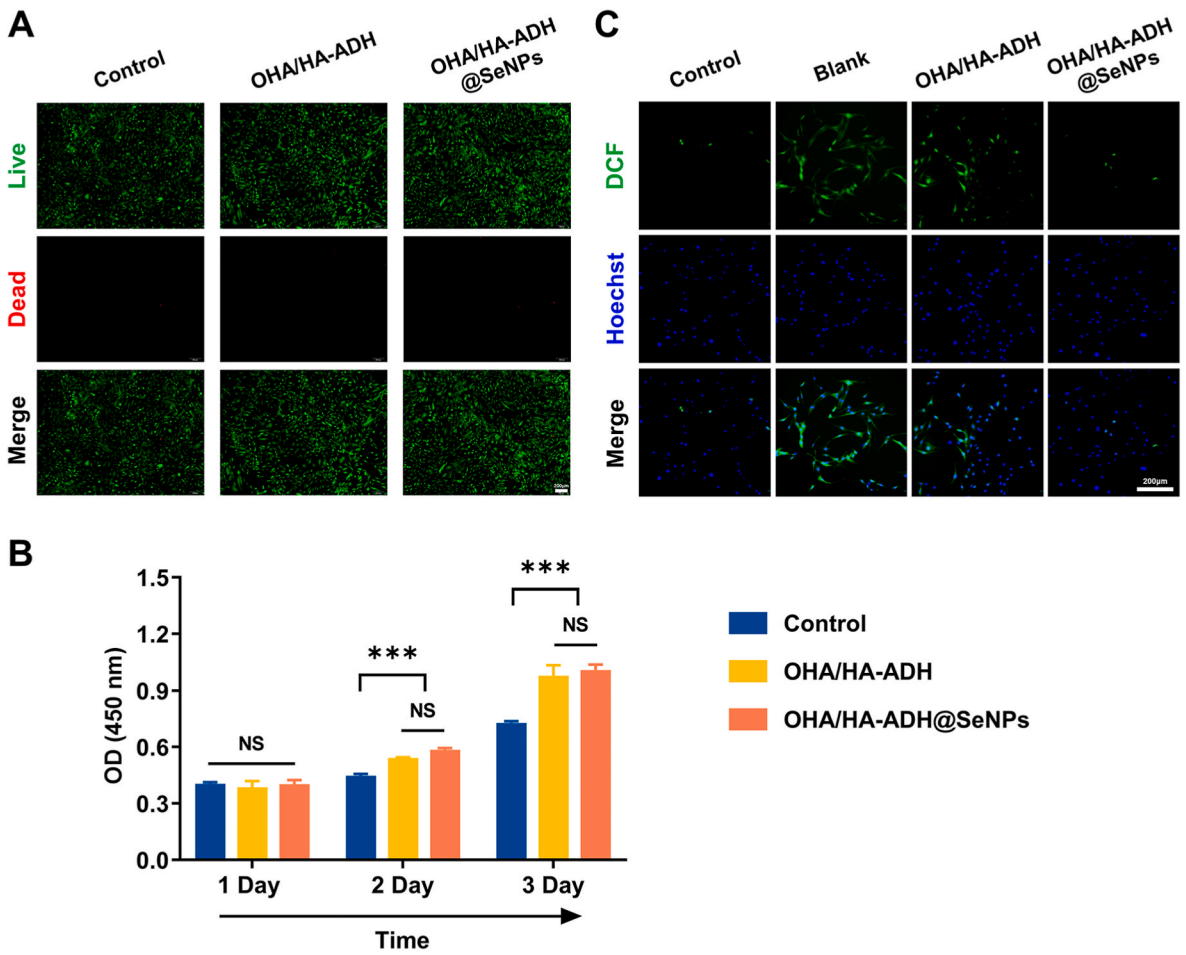

Fig. 3. Biocompatibility of OHA/HA-ADH@SeNPs-gels and antioxidative capacity of OHA/HA-ADH@SeNPs-gels *in vitro*. (A) Photographs of Live/Dead staining fluorescence. Scale bar = 200 μm. (B) The CCK-8 results on 3 days (n = 3, the results are shown as the mean ± SD. *, $p < 0.05$; **, $p < 0.01$; ***, $p < 0.001$). (C) Intracellular ROS-scavenging performance measured by DCF. Scale bar = 200 μm.

impact of OHA/HA-ADH@SeNPs on the level of biodegradation and synthesis imbalance of ECM, the protein expressions of MMP13 and COLII were significantly lower and higher, respectively, in the OHA/HA-ADH@SeNPs group than in the blank group (Fig. 4A–D). Similarly, RT-qPCR results was conducted and revealed that the expression of catabolic gene. The role of matrix metalloproteinase-13 (MMP13) was significantly reduced in the OHA/HA-ADH@SeNPs group than in the blank group (Fig. 4E). The expression of anabolic gene type II collagen (COLII) was significantly upregulated in the OHA/HA-ADH@SeNPs group than in the blank group (Fig. 4F). These outcomes indicated that the OHA/HA-ADH@SeNPs could suppress catabolic processes by delivering SeNPs.

It is widely thought that increased ROS levels can trigger apoptosis. The flow cytometry data showed that the number of apoptotic SW1353 cells was significantly less in the OHA/HA-ADH@SeNPs group than in the OHA/HA-ADH and blank groups (Fig. 4G), indicating that OHA/HA-ADH@SeNPs could maintain cellular homeostasis and inhibit apoptosis. The Live/Dead assay was then used to determine the effects of OHA/HA-ADH@SeNPs on pro-inflammatory cytokine IL-1β-induced SW1353 cells. As shown in Fig. 4H, the OHA/HA-ADH@SeNPs group had higher cell proliferation and fewer dead cells than OHA/HA-ADH and blank groups. Activation of the effector caspases-3 mediates regulated cell programmed apoptosis. Immunofluorescence staining was then applied to assess the cleaved caspase-3 expression. The OHA/HA-ADH@SeNPs group had a lower cleaved caspase-3 protein level (Fig. S10) than the OHA/HA-ADH and blank groups, indicating that OHA/HA-ADH@SeNPs could promote cell proliferation and improve cell survival under oxidative stress. In summary, OHA/HA-ADH@SeNPs hydrogels could scavenge ROS as brilliant antioxidant agents to maintain the balance of the antioxidant defense system. This could be ascribed to the combined effects of SeNPs and OHA/HA-ADH hydrogels.

3.6. *GPX1 modulation by OHA/HA-ADH@SeNPs contributes to oxidative stress suppression*

To comprehensively elucidate how OHA/HA-ADH@SeNPs regulated celluar redox homeostasis, given its selenium-responsive characteristics, the gene selected in this study was GPX1, which contains selenium and plays a pivotal role in antioxidant defense mechanisms (Fig. 5A) [21]. Previous studies have shown that GPX1-deficient mice had abnormalities in the myocardial vasculature due to susceptibility to oxidative stress after ischemia/reperfusion injury (IRI). Otherwise, a reduction in tissue damage caused by IRI could be achieved by overexpressing GPX1 [50]. Herein, the pathological changes in osteoarthritis were examined using articular cartilage harvested from patients undergoing knee arthroplasty. The cartilage tissues were found to have a reduced staining of acidic proteoglycans on histological analysis and elevated Osteoarthritis Research Society International (OARSI) scores (Fig. 5B and C). We found an overt reduction in GPX1 levels in severely injured articular cartilage (Fig. 5B and C). Subsequently, a reduction in GPX1 expression was observed *in vitro* as a result of proinflammatory stimuli. Remarkably, an upregulation of GPX1 levels was detected after OHA/HA-ADH@SeNPs treatment (Fig. 5D and F-G). Similar results were also found in DMM mice, in which the GPX1 levels in the articular cartilage were markedly

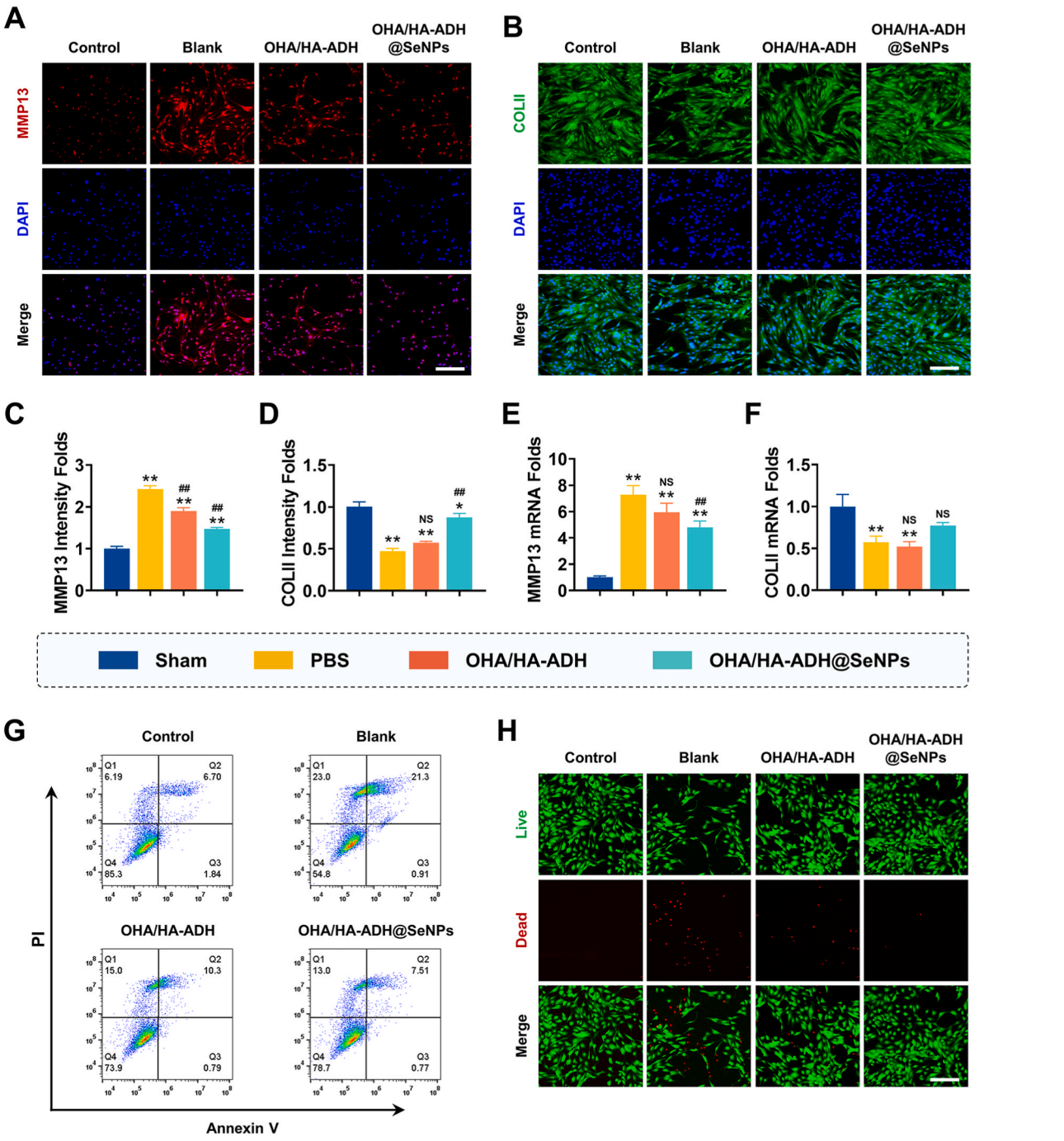

Fig. 4. Anti-catabolic and anti-apoptotic properties of the OHA/HA-ADH@SeNPs *in vitro*. (A) Immunofluorescence staining of MMP13 (the catabolic marker, red) and nuclei (blue). Scale bar = 200 μm. (B) Immunofluorescence staining of COLII (the anabolic marker, green) and nuclei (blue). Scale bar = 200 μm. (C–D) Quantification of MMP13 and COLII fluorescence. (E–F) The mRNA levels of MMP13 and COLII after treatment with or without OHA/HA-ADH@SeNPs, as evaluated by qRT-PCR analysis. (G) Cell apoptosis determined by Annexin V-APC/PI flow cytometry. (H) Cell death measured by Live/Dead assay. The scale bar is 200 μm. NS: meaningless, * and ** indicate $p < 0.05$, $p < 0.01$ when compared with the control group respectively, # and ## indicate $p < 0.05$, $p < 0.01$ when compared with the blank group respectively.

increased after OHA/HA-ADH@SeNPs treatment (Fig. 5E and H). Then, the intracellular glutathione peroxidase (GPX) level assay was performed to address the activity regulation of selenium-responsive protein of OHA/HA-ADH@SeNPs. The GPX activity in the blank group was significantly decreased, demonstrating the enzyme oxidizing system of chondrocytes was damaged under inflammation. The GPX activity of the administered groups (OHA/HA-ADH and OHA/HA-ADH@SeNPs) were significantly restored, especially the OHA/HA-ADH @SeNPs group (Fig. S11). To decipher the connection between GPX1 and oxidative stress, we suppressed GPX1 expression in SW1353 cells by siRNA (Fig. S12). Levels of ROS expression were found to be increased in normal cells upon GPX1 reduction, indicating that GPX1 could inhibit oxidative stress. Due to the induced expression of GPX1, the level of ROS was significantly lower in SW1353 cells exposed to OHA/HA-ADH@SeNPs than in cells without treatment (Fig. 5I and J). Collectively, these results indicated that GPX1 modulation contributed to the suppression of oxidative stress supperession by OHA/HA-ADH@SeNPs. In general, OHA/HA-ADH@SeNPs regulates the function of GPX1, including

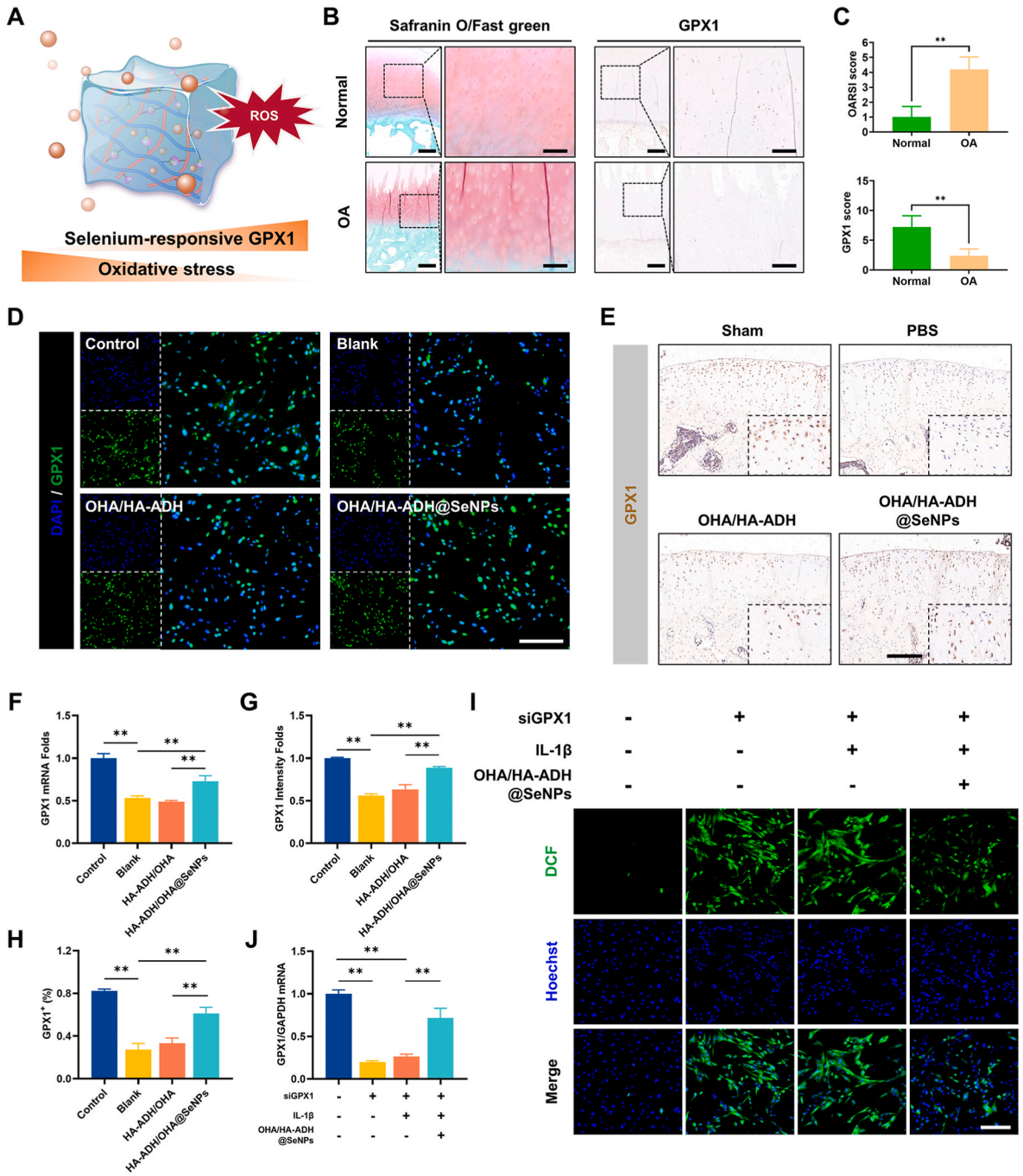

Fig. 5. GPX1 modulation by the OHA/HA-ADH@SeNPs contributes to oxidative stress suppression. (A) Schematic diagram of OHA/HA-ADH@SeNPs-driven redox reprogramming via selenium-responsive GPX1. (B) Safranin O/fast green staining of cartilage from the undamaged or damaged regions of human osteoarthritis cartilage. Scale bar, left, 500 μm; right, 200 μm. Immunohistochemistry assay with anti-GPX1 in the normal and osteoarthritis cartilage tissues. Scale bar, left, 500 μm; right, 200 μm. (C) The severity of cartilage destruction was evaluated by the OARSI grading system, and GPX1 scores in the undamaged or damaged regions of human osteoarthritis cartilage tissues were compared with the Mann-Whitney *U* test based on an immunohistochemistry assay. n = 5. (D) Immunofluorescence images of GPX1 (green) in SW1353 cells. Scale bar = 200 μm. (E) Immunohistochemical staining of GPX1 in articular cartilage. Scale bar, 200 μm. n = 5. (F) The GPX1 mRNA expression relative to GAPDH in SW1353 cells. (G) Quantification of GPX1 fluorescence. (H) Quantification of GPX1-positive chondrocytes. n = 3. (I) Measurement of intracellular ROS production by DCF. Scale bar, 200 μm. (J) qRT-PCR results showed the levels of GPX1. The results are shown as the mean ± SD. *, $p < 0.05$; **, $p < 0.01$.

promoting the expression and activity regulation of GPX1 [51]. These effects help to maintain intracellular redox balance and protect cells from oxidative stress damage.

3.7. OHA/HA-ADH@SeNPs-gel reduces articular space width narrowing, osteophyte formation, and subchondral bone sclerosis

To investigate the therapeutic effectiveness of OHA/HA-ADH@SeNPs-gel for osteoarthritis treatment, the surgical DMM rat model and exercise intervention were employed to induce osteoarthritis in the study (Fig. 6A and Fig. S13). PBS, OHA/HA-ADH-gel, or OHA/HA-ADH@SeNPs-gel were

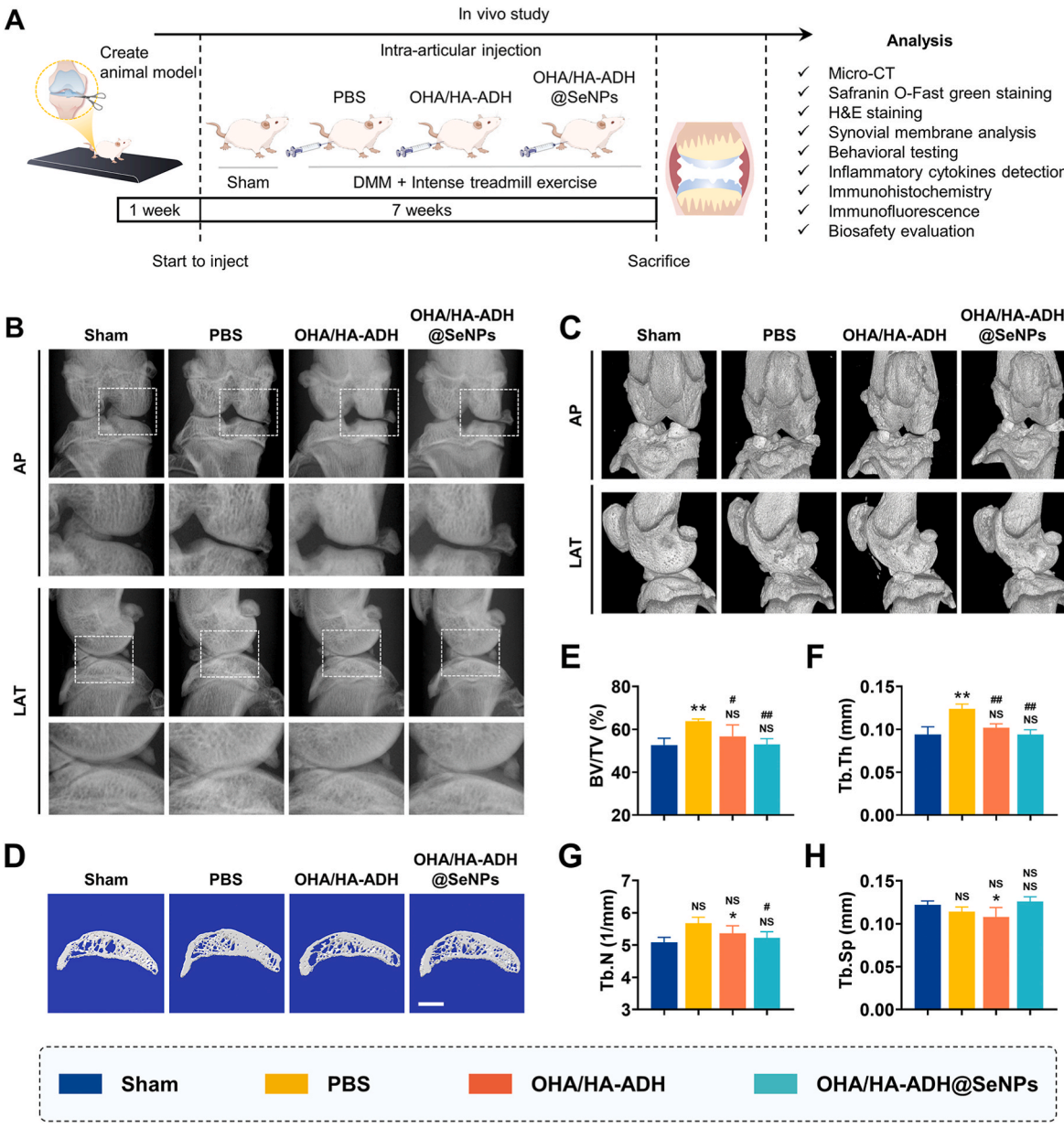

Fig. 6. Experimental group design, micro-CT analysis of knee joints. (A) Schematic illustration of establishment of the osteoarthritis rat model and the experimental design to evaluate the ameliorating effects of OHA/HA-ADH@SeNPs-gels. (B) Radiographs of the knee joint in AP and LAT view. (C) Micro-CT images of the knee joint in AP and LAT view. (D–H) Micro-CT reconstruction and quantitative analysis of medial subchondral bone. Scale bar, 500 μm. n = 5. NS: meaningless, * and ** indicate $p < 0.05$, $p < 0.01$ when compared with the sham group respectively, # and ## indicate $p < 0.05$, $p < 0.01$ when compared with the PBS group respectively.

given into the knee joint cavity of SD rats one week after they had undergone DMM surgery. Previous studies have reported that important pathological features of human osteoarthritis, such as joint space narrowing and osteophyte formation, are observed in animal models of osteoarthritis [52]. As shown in Fig. 6B and Fig. S14A significant decrease in joint space widths (JSW) was observed in the PBS and OHA/HA-ADH groups compared to the sham group. Contrastly, the OHA/HA-ADH@SeNPs group exhibited a more significant increase in the JSW more than the PBS group, indicating that OHA/HA-ADH@SeNPs could effectively mitigate cartilage degradation and preserve joint space. Additionally, osteophyte formation, another characteristic feature of osteoarthritis, was evaluated in this study [53]. The 3D stereo images were simulated according to the micro-CT scan. As shown in Fig. 6C, osteophyte formation was observed in the PBS, OHA/HA-ADH, and OHA/HA-ADH@SeNPs groups, while it was absent in the sham group. Moreover, the PBS group had significantly greater osteophyte formation than the OHA/HA-ADH@SeNPs group, indicating that OHA/HA-ADH@SeNPs could alleviate the formation of osteophytes and joint damage. Furthermore, OHA/HA-ADH@SeNPs administration reversed the uncoupled subchondral bone remodeling (Fig. 6D), as demonstrated by the improvements of trabecular thickness (Tb.Th), trabecular number (Tb.N), bone volume/total tissue volume (BV/TV), and trabecular bone separation (Tb.Sp) (Fig. 6E–H and Fig. S14B).

3.8. OHA/HA-ADH@SeNPs-gel ameliorates inflammation-induced pain-related behaviors

Osteoarthritis progression was associated with inflammation response and pain, inflammatory cytokines could sensitize nociceptive nerve terminals in synovium and induce inflammatory OA pain [6]. We observed that OHA/HA-ADH@SeNPs treatment alleviated the over-activated synovial inflammation (Fig. 7A–C). Meanwhile, as expected, OHA/HA-ADH@SeNPs-gel also additively suppress the expressions of

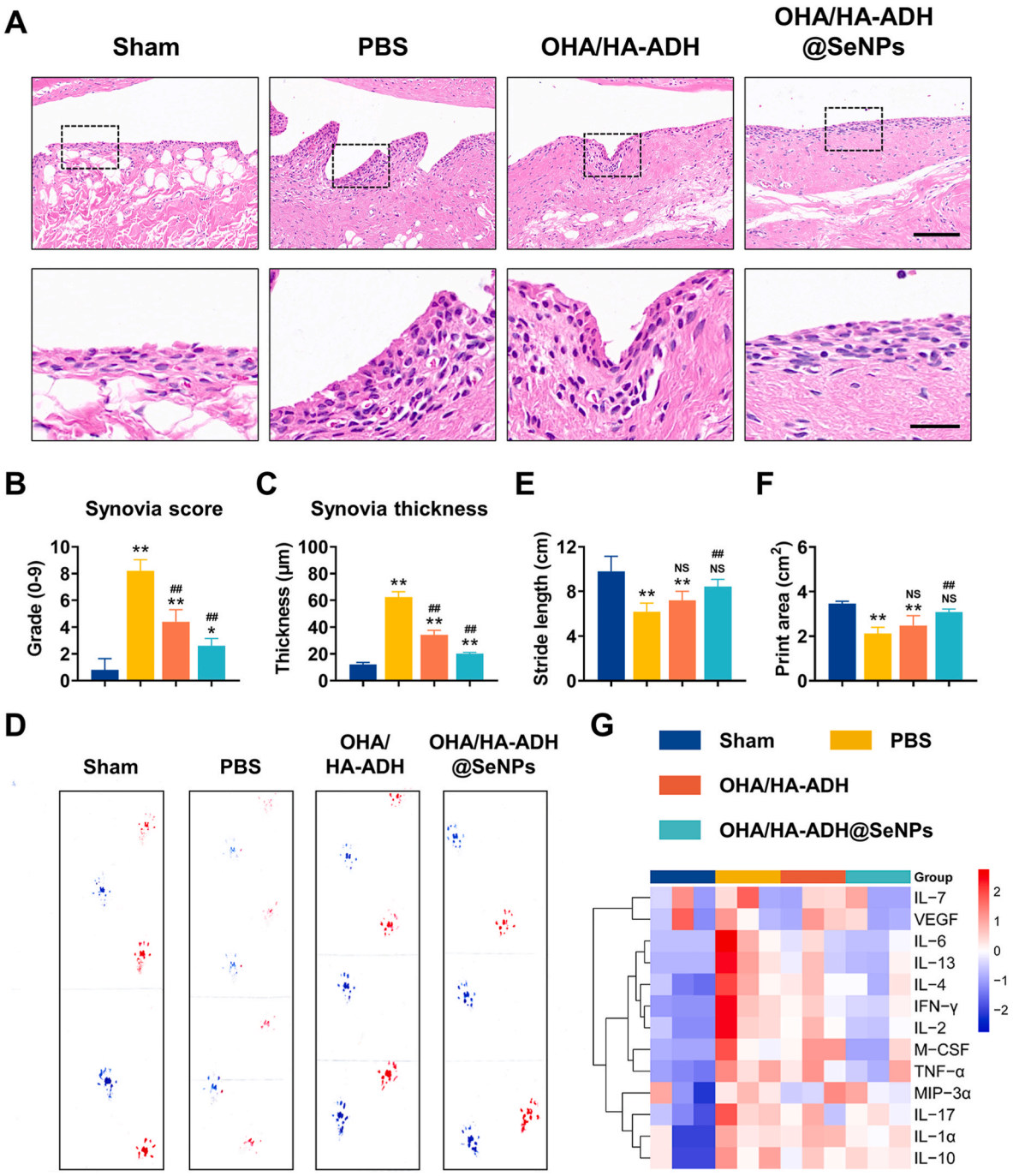

Fig. 7. Assessment of pain behavior and inflammatory response *in vivo*. (A–C) Staining of the synovium and quantitative analysis of inflammation in the synovium with H&E. Scale bar, 100 μm (top) and 25 μm (bottom). n = 5. (D) the footprints of rat 8 weeks after surgery. Red: modeling side, blue: healthy side. (E–F) Quantification of (E) footprints stride length and (F) footprints area. n = 5. NS: meaningless, * and ** indicate $p < 0.05$, $p < 0.01$ when compared with the sham group respectively, # and ## indicate $p < 0.05$, $p < 0.01$ when compared with the PBS group respectively. (G) Heatmap of the relative expression of inflammatory cytokines. Columns represent sample groups and rows represent cytokine species.

inflammatory cytokines over other treatments. The results of IHC staining showed that the percentages of tumor necrosis factor-α (TNF-α) and interleukin-1β (IL-1β) positive cells were significantly decreased in synovial tissues of the OHA/HA-ADH@SeNPs group compared to that of the PBS group (Figs. S15A–B). The mechanical pain of rats was detected using the von Frey filament stimulator (Fig. S16). As shown in Table S5, the PBS group displayed lower mechanical withdrawal threshold, whereas the mechanical withdrawal threshold (MWT) was particalaly relieved in rats treated with OHA/HA-ADH and further reduced after OHA/HA-ADH@SeNPs treatment, suggesting a successful analgesic effect. In addition, as shown in Fig. 7D, the footprints of each experimental group were collected 8 weeks after the operation. Subsequently, statistical analyses of the stride length and footprint area were performed on the collected footprints. These two parameters increased to varying degrees in the OHA/HA-ADH and OHA/HA-ADH@SeNPs groups compared with the PBS group, with the most significant increase in the latter group (Fig. 7E and F). Furthermore, to assess the long-term systemic inflammation after DMM surgery, the inflammatory cytokines were evaluated by antibody arrays and compared between groups. The results were rescaled to the range of features to scale the

range in [−1, 1] by min-max normalization and presented as a heatmap in Fig. 7G. The results showed that compared with the PBS group, the OHA/HA-ADH@SeNPs group lower serum levels of inflammatory factors (blue represented relatively low content, red represented relatively high content) after DMM surgery.

3.9. Structural degeneration of cartilage is attenuated by intra-articular injection of OHA/HA-ADH@SeNPs-gel

Subsequently, we used Safranin O-fast green and H&E staining to detect histological changes in the knee cartilage at 8 weeks post-operatively. As shown in Fig. 8A and B, in the PBS group, the articular cartilage showed weak Safranin O-fast green staining, severe surface abrasion, longitudinal fissure, erosive exfoliation, and disorganized chondrocytes. The morphological changes, tide line integrity, and matrix staining of the OHA/HA-ADH and OHA/HA-ADH@SeNPs groups were improved to varying degrees compared to those in the PBS group. In addition, compared with the scores of the PBS group, other treatment groups had different degrees of reduction, while the OHA/HA-ADH@SeNPs group showed a better treatment effect, as indicated by the OARSI score results shown in Fig. 8C and D. Other DMM-induced osteoarthritis symptoms, such as calcification of the articular cartilage zone and loss of hyaline cartilage were significantly reduced in the OHA/HA-ADH@SeNPs group.

As shown in Fig. 8E and G, a significant increase in MMP13 expression in articular cartilage was noted in the PBS, OHA/HA-ADH, and OHA/HA-ADH@SeNPs groups when compared with the sham group; however, among them, the increase in positive staining in the OHA/HA-ADH@SeNPs group was the smallest. In all treatment groups, the expression levels of COLII exhibited varying degrees of reduction compared to the sham operation group. Among them, the decrease in positive staining in the OHA/HA-ADH@SeNPs group was the smallest (Fig. 8F and H). In addition, terminal deoxynucleotidyl transferase dUTP nick end labeling (TUNEL) staining showed increased apoptosis in osteoarthritic chondrocytes in the PBS and OHA/HA-ADH@SeNPs groups compared with that in the sham group. Nevertheless, the OHA/HA-ADH@SeNPs reversed this pathological change (Fig. 8I). The percentage of apoptotic chondrocytes was significantly reduced in the OHA/HA-ADH@SeNPs group compared to the PBS group (Fig. 8J). The above results indicate that the OHA/HA-ADH@SeNPs could maintain cellular homeostasis and ameliorate apoptosis by releasing cartilage-targeting SeNPs-loaded hydrogel, thus alleviating joint wear and

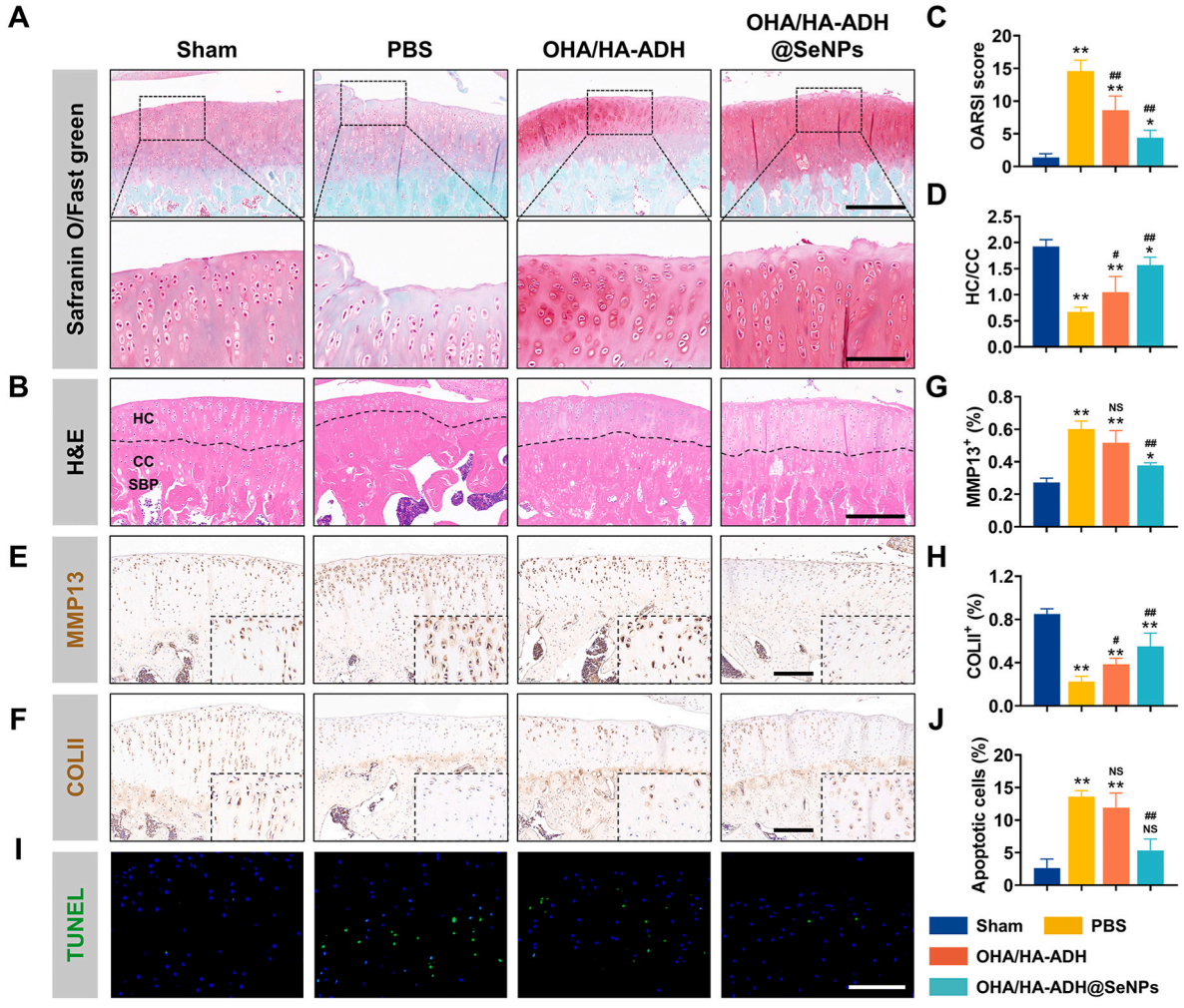

Fig. 8. Evaluation of cartilage repair *in vivo*. (A–B) Safranin O-fast green (upper) with the magnified area (bottom) in the boxed area in the upper image of joint sections at 8 weeks post-DMM. H&E staining with hyaline cartilage and calcified cartilage (separated by black dashed lines). Scale bar, top 300 μm; middle 100 μm; bottom 300 μm. (C–D) Quantitative analysis of medial tibial plateau joint scores based on the OARSI scoring system and the ratio of hyaline cartilage relative to the calcified cartilage. (E–F) Immunohistochemical staining of MMP13 and COLII in articular cartilage. Scale bar, 200 μm. The boxed area is enlarged in the bottom right corner. (G–H) Quantification of COLII- and MMP13-positive chondrocytes in cartilage. (I) Immunofluorescence staining of TUNEL. Scale bar, 100 μm. (J) Quantification of TUNEL-positive chondrocytes. n = 5. NS: meaningless, * and ** indicate $p < 0.05$, $p < 0.01$ when compared with the sham group respectively, # and ## indicate $p < 0.05$, $p < 0.01$ when compared with the PBS group respectively.

delaying the progression of osteoarthritis. In addition, the biocompatibility of the OHA/HA-ADH@SeNPs hydrogel was systematically assessed *in vivo*. Organ staining showed that the OHA/HA-ADH@SeNPs group was not observed to be different from the sham group, indicating that it had no potential *in vivo* toxicity (Fig. S17). Blood biochemical analysis showed that the typical liver and kidney function indicators of rats in all groups are within normal ranges (Figs. S18A–D). These results exhibited that the SeNPs released at the tissue site from hydrogel would not exert any systematic toxicity, demonstrating the extraordinary biocompatibility of the OHA/HA-ADH@SeNPs hydrogel *in vivo*, which holds great promise for treating osteoarthritis.

4. Conclusion

In summary, this study identified the significant role of selenium metabolism in osteoarthritis and revealed the specific alterations in selenoprotein expressions within the selenium metabolic pathway in chondrocytes under osteoarthritis conditions. Then, we developed a selenium rebalance-based hydrogel with self-healing capability, superior mechanical property, sustained SeNPs delivery through the mixture of OHA and HA-ADH by the dynamic equilibrium of Schiff base linkages. Importantly, the OHA/HA-ADH@SeNPs hydrogel could maintain cartilage homeostasis through the synergetic effects of scavenging ROS and depressing apoptosis *in vitro*. The results also demonstrated that the OHA/HA-ADH@SeNPs hydrogel could considerably ameliorate osteoarthritis symptoms *in vivo* in the DMM rat model. Specifically, it could ameliorate the development of osteoarthritis through a synergistic effect involving redox homeostasis restoration, and suppression of apoptosis and inflammatory profiles, to facilitate cartilage repair. As a powerful GPX1 activator and ROS scavenger, the OHA/HA-ADH@SeNPs hydrogels hold much promise for treating oxidative stress-related inflammatory diseases. Taken together, harnessing the OHA/HA-ADH@SeNPs hydrogel to address selenium imbalance demonstrates great potential as a promising approach for osteoarthritis treatment.

Credit author statement

Wenhui Hu: Methodology, Validation, Formal analysis, Investigation, Data curation, Writing – original draft, Writing – review & editing, Visualization. **Xuan Yao**: Methodology, Validation, Formal analysis, Investigation, Data curation, Writing – original draft, Writing – review & editing, Visualization. **Yuheng Li**: Supervision, Investigation. **Jianmei Li**: Investigation. **Jing Zhang**: Investigation. **Zhi Zou**: Investigation. **Fei Kang**: Investigation, Funding acquisition, Writing – review & editing. **Shiwu Dong**: Supervision, Funding acquisition, Writing – review & editing.

Declaration of competing interest

The authors declare that they have no known competing financial interests or personal relationships that could have appeared to influence the work reported in this paper.

Data availability

Data will be made available on request.

Acknowledgements

The authors are grateful for the funding provided for this study by the Key Programme of National Natural Science Foundation of China (81930067), Youth Program of National Natural Science Foundation of China (82002316), Chongqing Sports Research Project (B202333), Medical Innovation of Graduate Students in Chongqing (CYB23279), and General Program of Natural Science Foundation of Chongqing (cstc2019jcyj-msxmX0176).

Appendix A. Supplementary data

Supplementary data to this article can be found online at https://doi.org/10.1016/j.mtbio.2023.100864.

References

[1] B. Abramoff, F.E. Caldera, Osteoarthritis: pathology, diagnosis, and treatment options, Med. Clin. 104 (2) (2020) 293–311.
[2] Y. Jiang, Osteoarthritis year in review 2021: biology, Osteoarthritis Cartilage 30 (2) (2022) 207–215.
[3] R.N. Kalaria, R. Akinyemi, M. Ihara, Stroke injury, cognitive impairment and vascular dementia, Biochim. Biophys. Acta 1862 (5) (2016) 915–925.
[4] R. Liang, J. Zhao, B. Li, P. Cai, X.J. Loh, C. Xu, P. Chen, D. Kai, L. Zheng, Implantable and degradable antioxidant poly(ε-caprolactone)-lignin nanofiber membrane for effective osteoarthritis treatment, Biomaterials 230 (2020), 119601.
[5] O.M. Zahan, O. Serban, C. Gherman, D. Fodor, The evaluation of oxidative stress in osteoarthritis, Med Pharm Rep 93 (1) (2020) 12–22.
[6] P.G. Conaghan, A.D. Cook, J.A. Hamilton, P.P. Tak, Therapeutic options for targeting inflammatory osteoarthritis pain, Nat. Rev. Rheumatol. 15 (6) (2019) 355–363.
[7] P. Cao, Y. Li, Y. Tang, C. Ding, D.J. Hunter, Pharmacotherapy for knee osteoarthritis: current and emerging therapies, Expet Opin. Pharmacother. 21 (7) (2020) 797–809.
[8] L.M. Mancipe Castro, A.J. García, R.E. Guldberg, Biomaterial strategies for improved intra-articular drug delivery, J. Biomed. Mater. Res. 109 (4) (2021) 426–436.
[9] Q. Yao, X. Wu, C. Tao, W. Gong, M. Chen, M. Qu, Y. Zhong, T. He, S. Chen, G. Xiao, Osteoarthritis: pathogenic signaling pathways and therapeutic targets, Signal Transduct. Targeted Ther. 8 (1) (2023) 56.
[10] H. Li, M. Somiya, S. Kuroda, Enhancing antibody-dependent cellular phagocytosis by Re-education of tumor-associated macrophages with resiquimod-encapsulated liposomes, Biomaterials 268 (2021), 120601.
[11] S. Bastos Maia, A.S. Rolland Souza, M.F. Costa Caminha, S. Lins da Silva, R. Callou Cruz, C. Carvalho Dos Santos, M. Batista Filho, Vitamin A and pregnancy: a narrative review, Nutrients 11 (3) (2019) 681.
[12] C. Camaschella, Iron-deficiency anemia, N. Engl. J. Med. 372 (19) (2015) 1832–1843.
[13] V.M. Labunskyy, D.L. Hatfield, V.N. Gladyshev, Selenoproteins: molecular pathways and physiological roles, Physiol. Rev. 94 (3) (2014) 739–777.
[14] M.P. Rayman, Selenium and human health, Lancet 379 (9822) (2012) 1256–1268.
[15] L. Wang, J. Yin, B. Yang, C. Qu, J. Lei, J. Han, X. Guo, Serious selenium deficiency in the serum of patients with Kashin-Beck disease and the effect of nano-selenium on their chondrocytes, Biol. Trace Elem. Res. 194 (1) (2020) 96–104.
[16] N. Wang, M. Xie, G. Lei, C. Zeng, T. Yang, Z. Yang, Y. Wang, J. Li, J. Wei, J. Tian, T. Yang, A Cross-sectional study of association between plasma selenium levels and the prevalence of osteoarthritis: data from the Xiangya osteoarthritis study, J. Nutr. Health Aging 26 (2) (2022) 197–202.
[17] K. Zou, G. Liu, T. Wu, L. Du, Selenium for preventing Kashin-Beck osteoarthropathy in children: a meta-analysis, Osteoarthritis Cartilage 17 (2) (2009) 144–151.
[18] B. Kurz, B. Jost, M. Schünke, Dietary vitamins and selenium diminish the development of mechanically induced osteoarthritis and increase the expression of antioxidative enzymes in the knee joint of STR/1N mice, Osteoarthritis Cartilage 10 (2) (2002) 119–126.
[19] A. Khurana, S. Tekula, M.A. Saifi, P. Venkatesh, C. Godugu, Therapeutic applications of selenium nanoparticles, Biomed. Pharmacother. 111 (2019) 802–812.
[20] C. Ferro, H.F. Florindo, H.A. Santos, Selenium nanoparticles for biomedical applications: from development and characterization to therapeutics, Adv. Healthcare Mater. 10 (16) (2021), e2100598.
[21] S. Wang, Y. Chen, S. Han, Y. Liu, J. Gao, Y. Huang, W. Sun, J. Wang, C. Wang, J. Zhao, Selenium nanoparticles alleviate ischemia reperfusion injury-induced acute kidney injury by modulating GPx-1/NLRP3/Caspase-1 pathway, Theranostics 12 (8) (2022) 3882–3895.
[22] A. Raza, H. Johnson, A. Singh, A.K. Sharma, Impact of selenium nanoparticles in the regulation of inflammation, Arch. Biochem. Biophys. 732 (2022), 109466.
[23] Q. Chen, Y. Nan, Y. Yang, Z. Xiao, M. Liu, J. Huang, Y. Xiang, X. Long, T. Zhao, X. Wang, Q. Huang, K. Ai, Nanodrugs alleviate acute kidney injury: manipulate RONS at kidney, Bioact. Mater. 22 (2023) 141–167.
[24] X. Xiao, H. Deng, X. Lin, A.S.M. Ali, A. Viscardi, Z. Guo, L. Qiao, Y. He, J. Han, Selenium nanoparticles: properties, preparation methods, and therapeutic applications, Chem. Biol. Interact. 378 (2023), 110483.
[25] A. Mariano, I. Bigioni, F. Misiti, L. Fattorini, A. Scotto D'Abusco, A. Rodio, The nutraceuticals as modern key to achieve erythrocyte oxidative stress fighting in osteoarthritis, Curr. Issues Mol. Biol. 44 (8) (2022) 3481–3495.
[26] A. Sarrica, N. Kirika, M. Romeo, M. Salmona, L. Diomede, Safety and toxicology of magnolol and honokiol, Planta Med. 84 (16) (2018) 1151–1164.
[27] H. Zhang, S. Wu, W. Chen, Y. Hu, Z. Geng, J. Su, Bone/cartilage targeted hydrogel: strategies and applications, Bioact. Mater. 23 (2023) 156–169.
[28] S. Brown, S. Kumar, B. Sharma, Intra-articular targeting of nanomaterials for the treatment of osteoarthritis, Acta Biomater. 93 (2019) 239–257.
[29] J.S. Zhang, X.Y. Gao, L.D. Zhang, Y.P. Bao, Biological effects of a nano red elemental selenium, Biofactors 15 (1) (2001) 27–38.

[30] J. Zhang, X. Wang, T. Xu, Elemental selenium at nano size (nano-se) as a potential chemopreventive agent with reduced risk of selenium toxicity: comparison with Se-methylselenocysteine in mice, Toxicol. Sci. 101 (1) (2007) 22–31.
[31] S. Skalickova, V. Milosavljevic, K. Cihalova, P. Horky, L. Richtera, V. Adam, Selenium nanoparticles as a nutritional supplement, Nutrition 33 (2017) 83–90.
[32] Z. Cai, H. Zhang, Y. Wei, M. Wu, A. Fu, Shear-thinning hyaluronan-based fluid hydrogels to modulate viscoelastic properties of osteoarthritis synovial fluids, Biomater. Sci. 7 (8) (2019) 3143–3157.
[33] X. Cao, L. Sun, Z. Luo, X. Lin, Y. Zhao, Aquaculture derived hybrid skin patches for wound healing, Eng. Regen.n 4 (1) (2023) 28–35.
[34] D. Zhang, W. Li, Y. Shang, L. Shang, Programmable microfluidic manipulations for biomedical applications, Eng. Regen. 3 (2022) 258–261.
[35] Y. Gao, Q. Ma, Bacterial infection microenvironment-responsive porous microspheres by microfluidics for promoting anti-infective therapy, Smart Medicine (2022), e20220012.
[36] X. Lin, L. Cai, X. Cao, Y. Zhao, Stimuli-responsive silk fibroin for on-demand drug delivery, Smart Medicine 2 (2023), e20220019.
[37] D.Y. Kim, H. Park, S.W. Kim, J.W. Lee, K.Y. Lee, Injectable hydrogels prepared from partially oxidized hyaluronate and glycol chitosan for chondrocyte encapsulation, Carbohydr. Polym. 157 (2017) 1281–1287.
[38] C. Han, H. Zhang, Y. Wu, X. He, X. Chen, Dual-crosslinked hyaluronan hydrogels with rapid gelation and high injectability for stem cell protection, Sci. Rep. 10 (1) (2020), 14997.
[39] Y. Xiong, Z. Lin, P. Bu, T. Yu, Y. Endo, W. Zhou, Y. Sun, F. Cao, G. Dai, Y. Hu, L. Lu, L. Chen, P. Cheng, K. Zha, M.A. Shahbazi, Q. Feng, B. Mi, G. Liu, A whole-course-repair system based on neurogenesis-angiogenesis crosstalk and macrophage reprogramming promotes diabetic wound healing, Adv. Mater. (2023), e2212300.
[40] J. Chen, H. Zhu, Y. Zhu, C. Zhao, S. Wang, Y. Zheng, Z. Xie, Y. Jin, H. Song, L. Yang, J. Zhang, J. Dai, Z. Hu, H. Wang, Injectable self-healing hydrogel with siRNA delivery property for sustained STING silencing and enhanced therapy of intervertebral disc degeneration, Bioact. Mater. 9 (2022) 29–43.
[41] H. Ohzono, Y. Hu, K. Nagira, H. Kanaya, N. Okubo, M. Olmer, M. Gotoh, I. Kurakazu, Y. Akasaki, M. Kawata, E. Chen, A.C. Chu, K.A. Johnson, M.K. Lotz, Targeting FoxO transcription factors with HDAC inhibitors for the treatment of osteoarthritis, Ann. Rheum. Dis. 82 (2) (2023) 262–271.
[42] K. Xu, Y. He, S.A.A. Moqbel, X. Zhou, L. Wu, J. Bao, SIRT3 ameliorates osteoarthritis via regulating chondrocyte autophagy and apoptosis through the PI3K/Akt/mTOR pathway, Int. J. Biol. Macromol. 175 (2021) 351–360.
[43] F. Yu, X. Cao, J. Du, G. Wang, X. Chen, Multifunctional hydrogel with good structure integrity, self-healing, and tissue-adhesive property formed by combining diels–alder click reaction and acylhydrazone bond, ACS Appl. Mater. Interfaces 7 (43) (2015) 24023–24031.
[44] G.D. Prestwich, D.M. Marecak, J.F. Marecek, K.P. Vercruysse, M.R. Ziebell, Controlled chemical modification of hyaluronic acid: synthesis, applications, and biodegradation of hydrazide derivatives, J. Contr. Release 53 (1–3) (1998) 93–103.
[45] T. Kim, J. Suh, W.J. Kim, Polymeric aggregate-embodied hybrid nitric-oxide-scavenging and sequential drug-releasing hydrogel for combinatorial treatment of rheumatoid arthritis, Adv. Mater. 33 (34) (2021), e2008793.
[46] K.L. Pang, Y.Y. Chow, L.M. Leong, J.X. Law, N.A. Ghafar, I.N. Soelaiman, K.Y. Chin, Establishing SW1353 chondrocytes as a cellular model of chondrolysis, Life 11 (4) (2021) 272.
[47] E.N. Kim, H.S. Lee, G.S. Jeong, Cudratricusxanthone O inhibits H_2O_2-induced cell damage by activating Nrf2/HO-1 pathway in human chondrocytes, Antioxidants 9 (9) (2020) 788.
[48] C. Park, S.H. Hong, S.S. Shin, D.S. Lee, M.H. Han, H.J. Cha, S. Kim, H.S. Kim, G. Y. Kim, E.K. Park, Y.J. Jeon, Y.H. Choi, Activation of the Nrf2/HO-1 signaling pathway contributes to the protective effects of sargassum serratifolium extract against oxidative stress-induced DNA damage and apoptosis in SW1353 human chondrocytes, Int. J. Environ. Res. Publ. Health 15 (6) (2018) 1173.
[49] M.Y. Ansari, N. Ahmad, T.M. Haqqi, Oxidative stress and inflammation in osteoarthritis pathogenesis: role of polyphenols, Biomed. Pharmacother. 129 (2020), 110452.
[50] E. Lubos, N.J. Kelly, S.R. Oldebeken, J.A. Leopold, Y.Y. Zhang, J. Loscalzo, D. E. Handy, Glutathione peroxidase-1 deficiency augments proinflammatory cytokine-induced redox signaling and human endothelial cell activation, J. Biol. Chem. 286 (41) (2011) 35407–35417.
[51] Y. Zhao, H. Wang, J. Zhou, Q. Shao, Glutathione peroxidase GPX1 and its dichotomous roles in cancer, Cancers 14 (10) (2022) 2560.
[52] T. Paixao, M.D. DiFranco, R. Ljuhar, D. Ljuhar, C. Goetz, Z. Bertalan, H.P. Dimai, S. Nehrer, A novel quantitative metric for joint space width: data from the Osteoarthritis Initiative (OAI), Osteoarthritis Cartilage 28 (8) (2020) 1055–1061.
[53] J. Jamal, M.M. Roebuck, A. Wood, A. Santini, G. Bou-Gharios, S.P. Frostick, P. F. Wong, Histopathological dataset and demographic details of synovial tissues from patients with end-stage osteoarthritis, soft tissue and traumatic injuries of the knee, Data Brief 42 (2022), 108082.